

Characterization of the gate oxide of an AlGaN/GaN high electron mobility transistor

M. R. Holzworth,^{1,a)} N. G. Rudawski,¹ S. J. Pearton,¹ K. S. Jones,¹ L. Lu,² T. S. Kang,² F. Ren,² and J. W. Johnson³

¹Department of Materials Science and Engineering, University of Florida, Gainesville, Florida 32611-6400, USA

²Department of Chemical Engineering, University of Florida, Gainesville, Florida 32611-6400, USA

³Kopin Corporation, Taunton, Massachusetts 02780, USA

(Received 24 February 2011; accepted 3 March 2011; published online 21 March 2011)

A subnanometer thick interfacial oxide layer present between the Ni/Au gate metal stack and semiconducting epilayers of an AlGaN/GaN high electron mobility transistor was characterized using high-angle annular dark-field scanning transmission electron microscopy and laser-assisted atom probe tomography. It was revealed that the oxide is composed of distinct Ni-oxide-rich and Al-oxide-rich layers with no Ga-oxide detected. The results provide information that is of potential importance in determining failure mechanisms and improving reliability of AlGaN/GaN high electron mobility transistors. © 2011 American Institute of Physics. [doi:10.1063/1.3569715]

AlGaN/GaN high electron mobility transistors (HEMTs) exhibit excellent high frequency, high power, and high temperature performance and have the potential to replace Si- and GaAs-based transistors for a number of applications.¹⁻³ However, reliability and degradation issues remain as significant challenges to further device improvement.⁴⁻⁹ More specifically, interfacial layers between contacts and epilayers can have considerable effects on device performance. One particular area of concern is the interface between the gate metal stack and AlGaN epilayer. For example, it was shown that variations in Schottky barrier height (SBH) could be attributed to changes in interfacial layer thickness;¹⁰ device lifetime testing improved significantly when the interfacial layer was diminished. Therefore, accurate chemical characterization of the gate metal stack/AlGaN interfacial layer, which may have nm to subnanometer thickness, may prove crucial in understanding the defect formation mechanism(s) and ultimately improving HEMT reliability and performance. Here, a combination of high-angle annular dark-field scanning transmission electron microscopy (HAADF-STEM) and laser-assisted atom probe tomography (APT) were used to characterize a Ni/AlGaN interfacial oxide layer with subnanometer thickness.

The semiconducting epilayers in the AlGaN/GaN HEMTs used for this work were grown on 100-mm Si (111) substrates using metalorganic chemical vapor deposition with a scheme described elsewhere;^{3,10,11} the nominal composition of the AlGaN was Al_{0.26}Ga_{0.74}N. The fabrication steps following epilayer growth to create the HEMT structures (including Ni/Au gate metal stack Schottky contact formation) are described in detail in Ref. 2. The gate oxide of the devices was studied using HAADF-STEM and laser-assisted APT; samples were prepared using focused ion beam (FIB) milling methods described elsewhere.¹²⁻¹⁷ A HAADF-STEM image of the gate structure is presented in Fig. 1(a) with brighter features corresponding to areas of greater average atomic number; the individual Au, Ni, AlGaN, and

GaN layers are indicated along with the approximate area used for APT analysis. The high magnification HAADF-STEM image of the Ni/AlGaN interface presented in Fig. 1(b) indicates the detection of an interfacial layer (dark band) with subnanometer thickness; the darkness of the layer indicates it has light average atomic mass.

Laser-assisted APT was performed using an Imago local electrode atom probe (LEAP) 3000X-Si system; the addition of a pulsed laser allows the extension of APT from conductive to semi-insulating materials.^{12,17-22} During field evaporation, the specimen temperature was maintained at 65 K

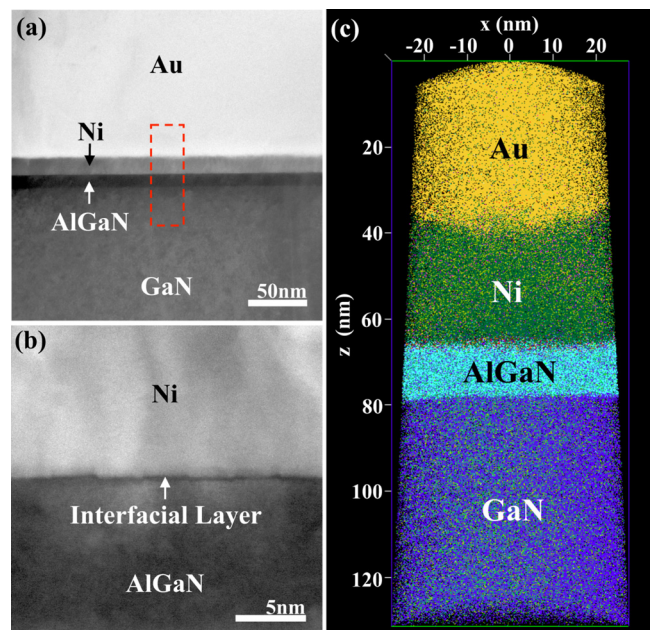


FIG. 1. (Color online) (a) HAADF-STEM image of the gate region of an AlGaN/GaN HEMT structure showing the distinct gate metal stack layers and semiconducting epilayers and (b) a high magnification HAADF-STEM image of the Ni/AlGaN interface, showing the presence of an interfacial layer. (c) Reconstructed APT data collected near gate metal stack/semiconducting epilayer interface displaying the distinct Au, Ni, AlGaN, and GaN layers. The boxed area in part (a) indicates the approximate area analyzed by APT as shown in (c).

^{a)}Author to whom correspondence should be addressed. Electronic mail: montaray@ufl.edu.

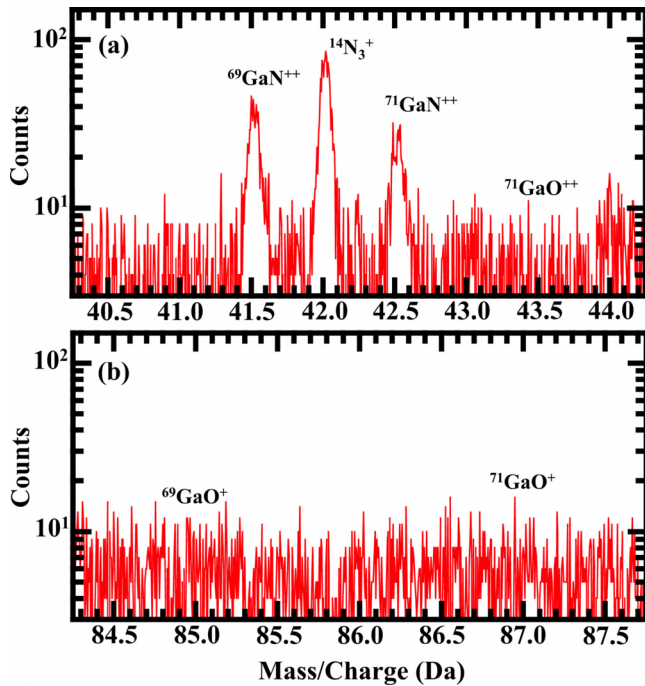


FIG. 2. (Color online) partial M/C spectra collected from APT analysis of the gate region of an AlGaIn/GaN HEMT structure: (a) from 40.5 to 44.0 indicating peaks at 41.5, 42.0, and 42.5 and (b) from 84.5 to 87.5 indicating no distinct peaks. The partial spectra are used to deduce a lack of Ga-oxide in the interfacial oxide.

with a chamber pressure $<3.2 \times 10^{-9}$ Pa, and the laser wavelength was 532 nm with a pulsing frequency of 250 kHz. Figure 1(c) presents a reconstruction of the collected data from a single APT sample showing the location of different individual atoms. The data reveals that the Ni/Au gate metal stack and AlGaIn/GaN epilayers were field evaporated in sequential order, therefore implying inclusion of the Ni/AlGaIn interfacial layer in the analysis.

The complete mass-to-charge (M/C) spectrum (not presented) of the region indicated in Fig. 1(a) indicates peaks at 21.5 and 74.0 that correspond to $^{27}\text{AlO}^{++}$ and $^{58}\text{NiO}^{+}$, respectively, which are presumably constituents of the interfacial oxide layer. A partial M/C spectrum shown in Fig. 2(a) shows three peaks at 41.5, 42.0, and 42.5; these peaks correspond to $^{69}\text{GaN}^{++}$, $^{14}\text{N}_3^{+}$, and $^{71}\text{GaN}^{++}$ or $^{69}\text{GaO}^{++}$, respectively. It is important to note there is no distinguishable peak at 43.5, which corresponds to $^{71}\text{GaO}^{++}$. Additionally, the partial M/C spectrum presented in Fig. 2(b) shows no distinctive peaks at 85.0 and 87.0, which correspond to $^{69}\text{GaO}^{+}$ and $^{71}\text{GaO}^{+}$, respectively.

The lack of a peak at 85.0 and the presence of a peak at 42.5 indicate the possibility that the peak at 42.5 may be due to $^{71}\text{GaN}^{++}$ instead of a $^{69}\text{GaO}^{++}$. Distinguishing between $^{71}\text{GaN}^{++}$ and $^{69}\text{GaO}^{++}$ can be accomplished by evaluating the isotopic ratio of $^{69}\text{Ga}/^{71}\text{Ga}$. If there is no significant amount of $^{69}\text{GaO}^{++}$ at the 42.5 peak, then the ratio of the value between the peaks at 41.5 and 42.5 should correspond to ratio between $^{69}\text{GaN}^{++}$ and $^{71}\text{GaN}^{++}$ which is correlated with the isotopic ratio between ^{69}Ga and ^{71}Ga , ~ 1.507 . Therefore, if a significant amount of $^{69}\text{GaO}^{++}$ is present, then the ratio between the peaks at 41.5 and 42.5 should be lower than the natural isotopic ratio.

The peaks at 41.5 and 42.5 are slightly non-Gaussian in shape; instead of possessing a true, center maximum, each

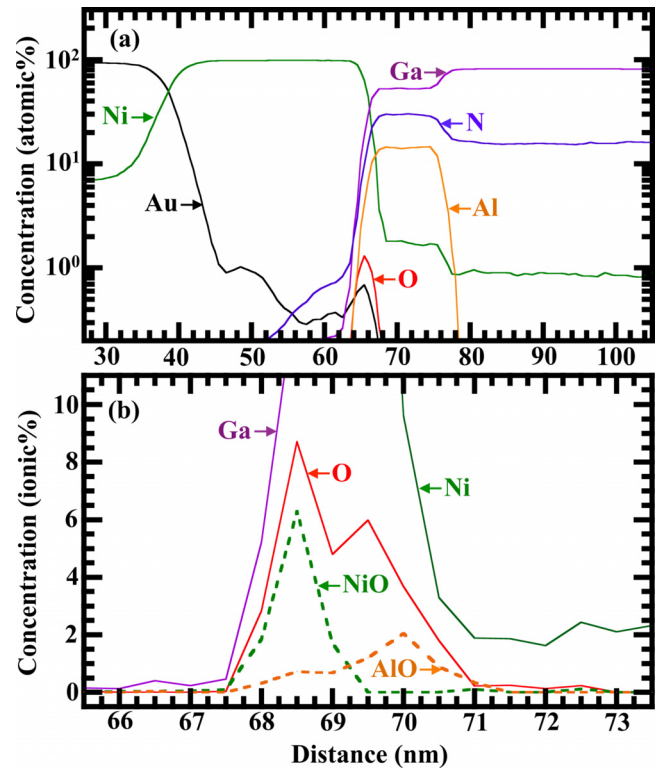


FIG. 3. (Color online) (a) The complete 1D atomic concentration profile for the gate region of the HEMT indicating an O peak at the Ni/AlGaIn interface and (b) 1D ionic concentration profiles of O^{+} , $^{27}\text{AlO}^{++}$, and $^{58}\text{NiO}^{+}$ measured in the vicinity of the interfacial layer indicating the oxide is composed of distinct AlO_x and NiO_x layers.

peak has a slight plateau where there are multiple maximums that may or may not be centered. To compensate for this shape, the average value over the plateau was calculated and used as the number of counts at the 41.5 and 42.5 peaks. The average ratio between the peaks at 41.5 and 42.5 was calculated to be 1.516 ± 0.05 ; this value is within measurement error of the natural isotopic ratio of ^{69}Ga to ^{71}Ga . With the measured ratio very close to the natural isotopic ratio, it is reasonably concluded that 42.5 is most likely a $^{71}\text{GaN}^{++}$ peak instead of a $^{69}\text{GaO}^{++}$ peak. Thus, with the peak at 42.5 associated with $^{71}\text{GaN}^{++}$, there appears to be no GaO_x detected in the HEMT.

One-dimensional (1D) concentration profiles of Au, Ni, O, Ga, N, and Al across the gate region into the semiconducting epilayers were obtained from the full reconstruction presented in Fig. 1(c) using a 40 nm cylindrical data pipe. The data pipe was positioned orthogonally to the Ni/AlGaIn interface by using the isoconcentration curve of Al. By positioning the data pipe orthogonal to the interface, the resulting 1D concentration profile is more accurate because the smearing between the layers is minimized. The complete 1D atomic concentration profile for the gate region of the HEMT is shown in Fig. 3(a) indicating an O peak at the Ni/AlGaIn interface, confirming the evaporated O^{+} detected in the full M/C spectrum resides in the Ni/AlGaIn interfacial layer. Peaks on the full M/C spectrum at 21.5 and 74.0 were previously identified as $^{27}\text{AlO}^{++}$ and $^{58}\text{NiO}^{+}$; the 1D concentration profiles of these ions are presented in Fig. 3(b) in addition to the measured O^{+} profile in the interfacial layer. The peaks of the $^{27}\text{AlO}^{++}$ and $^{58}\text{NiO}^{+}$ ions are distinct and do not overlap within the O^{+} profile indicating the interfacial layer

is composed of distinct AlO_x and NiO_x layers adjacent to the AlGaIn epilayer and Ni gate contact, respectively.

The observation that the interfacial oxide is composed of distinct NiO_x and AlO_x layers is an important result and provides insight into possible device failure mechanisms. Specifically, it is known that AlGaIn oxidation can occur even under ultrahigh vacuum conditions,²³ and the oxidized layer consists of nonstoichiometric O-rich AlO_x .^{24–27} The excess O from the AlO_x layer can therefore be used to form an adjacent NiO_x layer during or after Ni deposition, which changes the composition of the AlO_x layer. The generation of the NiO_x layer and/or the compositional changes to the AlO_x layer after NiO_x generation may change the electrical properties of the gate/channel interface, particularly the surface Fermi level, SBH, and surface band bending, which will influence device performance and may influence device failure. While this proposed formation mechanism is speculative, accurate characterization of the interfacial oxide is an important step in avoiding its formation.

In conclusion, HAADF-STEM and laser-assisted APT were used to study a subnanometer interfacial oxide layer between a Ni/Au gate metal stack and AlGaIn/GaN epilayer in a HEMT device. It was determined that the layer contains no GaO_x and apparently consists of distinct AlO_x and NiO_x layers adjacent to the AlGaIn epilayer and Ni gate metal, respectively. Furthermore, characterization of the interfacial oxide provides information that could potentially be used to improve device reliability and performance.

The authors acknowledge the Air Force Office of Scientific Research and the Multidisciplinary Research Initiative for funding this research, the Major Analytical Instrumentation Center at the University of Florida for use of the TEM and FIB facilities, the Central Analytical Facility at the University of Alabama for the use of the LEAP facilities, and Dr. Paul Holloway, Dr. Brent Gila, and Rich Martens for fruitful discussion on many issues.

¹M. Feng, S. Shyh-Chiang, D. C. Caruth, and J. J. Huang, *Proc. IEEE* **92**, 354 (2004).

²J. W. Johnson, E. L. Piner, A. Vescan, R. Therrien, P. Rajagopal, J. C. Roberts, J. D. Brown, S. Singhal, and K. J. Linthicum, *IEEE Electron Device Lett.* **25**, 459 (2004).

³W. Nagy, J. Brown, R. Borges, and S. Singhal, *IEEE Trans. Microwave Theory Tech.* **51**, 660 (2003).

⁴C.-Y. Chang, T. Anderson, J. Hite, L. Lu, C.-F. Lo, B.-H. Chu, D. J.

Cheney, E. A. Douglas, B. P. Gila, F. Ren, G. D. Via, P. Whiting, R. Holzworth, K. S. Jones, S. Jang, and S. J. Pearton, *J. Vac. Sci. Technol. B* **28**, 1044 (2010).

⁵U. Chowdhury, J. L. Jimenez, C. Lee, E. Beam, P. Saunier, T. Balistreri, P. Seong-Yong, L. Taehun, J. Wang, M. J. Kim, J. Jungwoo, and J. A. del Alamo, *IEEE Electron Device Lett.* **29**, 1098 (2008).

⁶J. A. del Alamo and J. Joh, *Microelectron. Reliab.* **49**, 1200 (2009).

⁷E. A. Douglas, C. Y. Chang, D. J. Cheney, B. P. Gila, C. F. Lo, L. Lu, R. Holzworth, P. Whiting, K. Jones, G. D. Via, J. Kim, S. Jang, F. Ren, and S. J. Pearton, *Microelectron. Reliab.* **51**, 207 (2011).

⁸J. Joh and J. A. del Alamo, *IEEE Electron Device Lett.* **29**, 287 (2008).

⁹S. Y. Park, C. Floresca, U. Chowdhury, J. L. Jimenez, C. Lee, E. Beam, P. Saunier, T. Balistreri, and M. J. Kim, *Microelectron. Reliab.* **49**, 478 (2009).

¹⁰S. Singhal, T. Li, A. Chaudhari, A. W. Hanson, R. Therrien, J. W. Johnson, W. Nagy, J. Marquart, P. Rajagopal, J. C. Roberts, E. L. Piner, I. C. Kizilyalli, and K. J. Linthicum, *Microelectron. Reliab.* **46**, 1247 (2006).

¹¹J. D. Brown, R. Borges, E. Piner, A. Vescan, S. Singhal, and R. Therrien, *Solid-State Electron.* **46**, 1535 (2002).

¹²B. P. Gorman, A. G. Norman, and Y. Yan, *Microsc. Microanal.* **13**, 493 (2007).

¹³D. J. Larson, D. T. Foord, A. K. Petford-Long, T. C. Anthony, I. M. Rozdilsky, A. Cerezo, and G. W. D. Smith, *Ultramicroscopy* **75**, 147 (1998).

¹⁴M. K. Miller, K. F. Russell, and G. B. Thompson, *Ultramicroscopy* **102**, 287 (2005).

¹⁵M. K. Miller, K. F. Russell, K. Thompson, R. Alvis, and D. J. Larson, *Microsc. Microanal.* **13**, 428 (2007).

¹⁶G. B. Thompson, M. K. Miller, and H. L. Fraser, *Ultramicroscopy* **100**, 25 (2004).

¹⁷K. Thompson, P. L. Flaitz, P. Ronsheim, D. J. Larson, and T. F. Kelly, *Science* **317**, 1370 (2007).

¹⁸M. J. Galtrey, R. A. Oliver, M. J. Kappers, C. J. Humphreys, D. J. Stokes, P. H. Clifton, and A. Cerezo, *Appl. Phys. Lett.* **90**, 061903 (2007).

¹⁹K. Inoue, F. Yano, A. Nishida, H. Takamizawa, T. Tsunomura, Y. Nagai, and M. Hasegawa, *Appl. Phys. Lett.* **95**, 043502 (2009).

²⁰M. Kodzuka, T. Ohkubo, K. Hono, F. Matsukura, and H. Ohno, *Ultramicroscopy* **109**, 644 (2009).

²¹J. S. Moore, K. S. Jones, H. Kennel, and S. Corcoran, *Ultramicroscopy* **108**, 536 (2008).

²²D. E. Perea, E. R. Hemesath, E. J. Schwalbach, J. L. Lensch-Falk, P. W. Voorhees, and L. J. Lauhon, *Nat. Nanotechnol.* **4**, 315 (2009).

²³B. Boudjelida, M. C. Simmonds, I. Gee, and S. A. Clark, *Appl. Surf. Sci.* **252**, 5189 (2006).

²⁴N. V. Edwards, M. D. Bremser, J. T. W. Weeks, R. S. Kern, R. F. Davis, and D. E. Aspnes, *Appl. Phys. Lett.* **69**, 2065 (1996).

²⁵T. Hashizume, S. Ootomo, S. Oyama, M. Konishi, and H. Hasegawa, *J. Vac. Sci. Technol. B* **19**, 1675 (2001).

²⁶T. Hashizume, S.-y. Ootomo, R. Nakasaki, S. Oyama, and M. Kihara, *Appl. Phys. Lett.* **76**, 2880 (2000).

²⁷X. L. Wang, D. G. Zhao, J. Chen, X. Y. Li, H. M. Gong, and H. Yang, *Appl. Surf. Sci.* **252**, 8706 (2006).